# Reappraising the production and transfer of hydrogen atoms from the middle to the upper atmosphere of Mars at times of elevated water vapor

**F. Montmessin[1], D. A. Belyaev[2], F. Lefèvre[3], J. Alday[4,6], M. Vals[1], A. A. Fedorova[2], O. I. Korablev[2], A. V. Trokhimovskiy[2], M. S. Chaffin[5], N. M. Schneider[5]**

[1]LATMOS/IPSL, UVSQ Université Paris-Saclay, Sorbonne Université, CNRS, Guyancourt, France.

[2]Space Research Institute of the Russian Academy of Sciences (IKI RAS), Moscow, Russia, Sorbonne

[3]LATMOS/IPSL, Sorbonne Université, UVSQ Université Paris-Saclay, CNRS, Paris, France.

[4z]Physics Department, Oxford University, Oxford, United Kingdom.

[5]Laboratory for Atmospheric and Space Physics, Boulder, Colorado, United States

[6]School of Physical Sciences, The Open University, Milton Keynes, United Kingdom

Corresponding author. Email: franck.montmessin@latmos.ipsl.fr

**Key Points:**

- We decipher hydrogen production and migration to Mars' upper atmosphere using a box model for a variety of elevated water vapor cases
- H atoms formed between 60 and 80 km supply a dominant fraction of hydrogen to the upper atmosphere
- Our results suggest that perihelion climate dominates hydrogen transfer to the upper atmosphere overall

**Abstract**

Water escape on Mars has recently undergone a paradigm shift with the discovery of unexpected seasonal variations in the population of hydrogen atoms in the exosphere where thermal escape occurs and results in water lost to space. This discovery led to the hypothesis that, contradicting the accepted pathway, atomic hydrogen in the exosphere was not only produced by molecular hydrogen but mostly by high altitude water vapor. Enhanced presence of water at high altitude during southern spring and summer, due to atmospheric warming and intensified transport, favors production of H through photolysis ionized chemistry of water molecules and thus appears to be the main cause of the observed seasonal variability in escaping hydrogen. This hypothesis is supported by the observation of large concentrations of water vapor between 50 km and 150 km during the southern summer solstice and global dust events. Using a simplified yet representative air parcel transport model, we show that in addition to the formation of atomic hydrogen from water photolysis above 80 km, a major fraction of the exospheric hydrogen is formed at altitudes as low as 60 km and is then directly advected to the upper atmosphere. Comparing the injection modes of a variety of events (global dust storm, perihelion periods, regional storm), we conclude that southern spring/summer controls H production and further ascent into the upper atmosphere on the long term with direct implication for water escape.

**Plain language Summary**

Numerous lines of evidence suggest that Mars' water inventory was much larger in the past than it is today. The loss of this inventory has been driven by the formation of hydrated minerals on the surface, as well as by the escape of water to space. The first part of the escape process comprises the formation of H atoms, which may escape the planet once they reach the uppermost layers of the atmosphere. Here, we investigate one mechanism by which the H atoms may reach these high altitudes: the breakdown of water molecules by solar ultraviolet photons in the middle atmosphere (60-70 km above the surface), and the posterior ascent of the newly formed H atoms to the upper altitudes. We use a model that reveals that this process is the dominant contributor of atomic H to the upper atmosphere during periods of strong atmospheric circulation. In particular, we find that this mechanism is most efficient during the spring/summer season in the Southern Hemisphere, when Mars is closest to the Sun. Given that this season occurs every Martian year, our calculations suggest that this process has been the dominant contributor to water escape in the long term.

## 1 Introduction

Mars has probably lost to space a large part of its initial inventory of water and carbon dioxide (Jakosky et al., 2018) in addition to water trapped in hydrated minerals (Scheller et al., 2021). Indeed, the scars left at the surface by a previously widespread and active liquid water cycle (Carr, 1987) imply that massive amounts of water and carbon dioxide have disappeared from the planet over the ages, consequently making the presumably warm and wet primitive climate progressively transition during the last three billion years to the cold, and hyper arid climate that prevails nowadays.

Several studies conducted in the last decades have tried to unveil the main cause of the demise of primordial Martian water. The studies considered that a simple and still active loss mechanism is maintained indirectly by the thermal escape of hydrogen atoms in the exosphere, i.e., above an altitude of 200 km, a region where they are observed to populate the outer fringes of the atmosphere and to interact with the space environment. The theory underlying water escape has received considerable attention, as new evidence collected since 2014 have revealed major deficiencies in our initial understanding of the main mechanism controlling escape.

### 1.1 Water escape: from theory to observations

Water vapor is the main hydrogen carrier in the lower atmosphere of Mars. It is sourced from the massive icy deposits at the poles, which sublime in spring and summer. The conversion of water vapor in the lower atmosphere into the upper atmosphere hydrogen was initially thought to be a sluggish process paced by the formation of $H_2$ molecules out of $H_2O$ dissociation (McElroy & Donahue 1972, Parkinson and Hunten, 1972). While H atoms are produced everywhere in the column, they are short lived in the lower atmosphere and cannot move away from their source region. In contrast, $H_2$ has a centuries long lifetime and can access the ionosphere (>100 km) where it reacts with $CO_2^+$ and releases H (Krasnopolsky, 2002).

The key reason that explains why only $H_2$ is involved in this indirect hydrogen transfer to the upper atmosphere is that $H_2$ is not bound to condense like water is in the atmosphere. On Mars, temperature conditions make water vapor saturate at an altitude that varies with seasons and latitude, but generally lies between near the surface and the upper troposphere (above 40 km). This saturation level, also referred to as the hygropause or cold trap, is supposed to cap the bulk of water vapor and confine it below. Above, water vapor sharply declines, as any water molecule exceeding vapor pressure should turn to ice. Once this vapor excess is converted into water ice cloud particles, its higher density as a solid makes it fall and release water vapor below the condensation level, sequestering water there. The initial theory for the upper H production therefore relied on the idea that, with a hygropause level being so low, water vapor alone could not be a significant carrier of H to the upper atmosphere, leaving the long-lived $H_2$ handling most of this transfer.

The sequestration effect of hygropause on water vapor profile was discussed first by Davies (1979) and later evidenced by ground-based observations (Clancy et al., 1996) and the Phobos 2 mission using solar occultation in the infrared (Rodin et al., 1997). These observations led Clancy et al. (1996) to speculate about the long-term consequences of this sequestration below the hygropause. The authors argued that the colder aphelion climate should favor the retention of water in the spring/summer Hemisphere of Mars, that is, the Northern Hemisphere whose pole exposes the largest reservoir of ice.

Regardless of its consequences for the mobilization of the surface ice reservoir, the hygropause level has also been regarded as preventing the transfer of water to the upper atmosphere. Yet, the $H_2$-driven production theory has not withstood the Martian corona observations of SPICAM on Mars Express and Hubble Space Telescope that revealed unexpected changes in its brightness on a few weeks' timescale (Chaffin et al., 2014; Clarke et al., 2014). Such rapid changes are incompatible with the centuries-long steady production of H atoms imparted by $H_2$, which thus called for a different or additional source. The fact that enhanced coronal brightness occurred during the 2007 Global Dust Storm (GDS) led Chaffin et al. (2014) to propose that an increase in high altitude water at that time could explain the intensification of H production, and be the main contributor of water lost to space over the long term. Details on how water could become the main contributor of H were presented in Chaffin et al. (2017) who modeled the effect of water plumes deposited at a variety of altitudes from 20 to 120 km and showed how fast and strong the plumes turned into an enhanced production of H atoms. The main conclusion in that study is that if sufficient water is brought up to a level where photodissociation dominates the production of H (that is above 60 km), then a rapid response is predicted for H production and escape with rates drastically changing in a timescale of weeks, therefore explaining how the Martian corona could have been observed to vary on comparable timescales. Enhanced water presence above 60 km was reported by several authors (Maltagliati et al., 2013; Fedorova et al., 2018), thereby establishing the link between enhanced high altitude water vapor and enhanced exospheric hydrogen.

Numerous other works have followed this study and attempted to refine these initial results (Heavens et al. 2018, Krasnopolsky, 2019; Fedorova et al. 2020; Stone et al. 2020; Fedorova et al. 2021; Chaffin et al. 2021) to address the respective contributions of isolated events (global or regional dust storms) and the global increase in dust and temperature that occurs annually around perihelion, i.e., at the transition between the southern spring and summer. Further, Krasnopolsky (2019) and Stone et al. (2020) also demonstrated that ionized chemistry can efficiently decompose high altitude water into escaping H atoms.

These studies provide complementary insights into the efficiency with which ionized and neutral chemistry converts high-altitude water vapor into escaping hydrogen. They endorse the idea that, on an annual basis, hydrogen thermal escape is primarily driven by the increased presence of water vapor above 60 km, which only occurs during southern spring and summer.

### 1.2 Observations of water vapor vertical distribution

Water vapor vertical distribution has long remained a missing product of Mars' observations. Until recently, the SPICAM infrared spectrometer onboard Mars Express has been the only asset to regularly survey water vapor vertical distribution (Fedorova et al., 2009; 2018; 2021; Maltagliati et al., 2011; 2013) using solar occultation mode, a technique that provides both sensitive (between 1 and 10 parts-per-million in volume, ppmv, in $H_2O$ volume mixing ratio, vmr) and vertically resolved (3 to 5 km vertical sampling) measurements. The enhanced presence of water vapor at high altitude during southern summer was already evidenced in some of these works, but SPICAM occultation coverage is hampered by Mars Express highly elliptical orbit, forcing an uneven temporal and latitudinal sampling, as well as by its limited detection capability.

With the advent of the Trace Gas Orbiter in 2018, water vapor profiles have been explored with far better accuracy and coverage through the use of state-of-the-art infrared spectrometers allowing for one to two orders better spectral resolution and sensitivity than SPICAM and taking advantage of the TGO orbit to optimize latitude/time coverage. The first surveys of water vapor accomplished by the Atmospheric Chemistry Suite (ACS) and the Nadir and Occultation for Mars Atmosphere Discovery (NOMAD) (Vandaele et al., 2019; Aoki et al., 2019; Fedorova et al., 2020) have set a new standard in profiling water, especially during southern spring and summer and also allowed for a comparison between a regular year and a year marked by a global dust storm (GDS). In particular, Belyaev et al. (2021) were able to profile, for the first time, water vapor up to 120 km using the strong water band at 2.6 μm sampled by the ACS instrument. In addition to TGO, the Neutral Gas and Ions Mass Spectrometer (NGIMS) onboard the Mars Atmosphere and Volatile EvolutioN (MAVEN) has sampled *in situ* the ion composition of the atmosphere above 150 km and occasionally down to 120 km during deep dips, allowing for indirect identification and quantification of water vapor in the thermosphere (Stone et al., 2020).

Together, TGO and MAVEN have revealed several striking features about water vapor. First, at times of dust storms which occur in the second half of the Martian year, water is observed to propagate up to >100 km and persists there for several months before disappearing by the end of the year. Not only is it observed at altitudes that were not anticipated, but it is also observed there to be in substantial quantity (i.e., 20 ppmv at 120 km, Belyaev et al., 2021), at odds with what one may expect from a hygropause-dominated water vapor profile. In addition, ACS, which can probe water vapor abundance and measure atmospheric temperature from the same measurement, has documented remarkably large amounts of water in excess of saturation between 60 and 80 km (saturation ratio >10, Fedorova et al., 2020), demonstrating the very high porosity of the hygropause and thus its reduced ability to sequester water below.

Finally, the dense temporal sampling of NGIMS has also shown that water transfer to the middle thermosphere (150 km) has a characteristic timescale of the order of days, with concentrations tripling in a few days (Stone et al., 2020).

In summary, southern summer water vapor relies on a unique combination of favorable factors (rapid transport, warm atmosphere, little to no hygropause effect) to swiftly penetrate the upper atmosphere and deliver hydrogen atoms that are subsequently released. However, the transfer of hydrogen atoms directly from their bulk source region in the middle atmosphere has never been addressed through the perspective of vertical advection that prevails during these high water events (Shaposhnikov et al., 2022) and whose nature contrasts with diffusive transport.

## 2 Model

Chaffin et al. (2017) have revealed the importance of hydrogen atom formation and transport in and from the region between 60 and 80 km, yet their model idealized the presence of water vapor at high altitudes and represented transport as a diffusive process which, by definition, ignores the unidirectional nature of advection whose strength does not depend on the tracer gradient. Such a representation of transport was also employed by Krasnopolsky (2019) who only considered the atmosphere above 80 km and specified a boundary condition for water vapor abundance at the bottom of his model. None of these studies therefore relied on a faithful representation of atmospheric transport, nor did they rely on the detailed observations of water vapor profiles that have been produced by TGO since then. These results were then analyzed using Martian GCMs, where NOMAD, ACS and MCS data were tentatively reproduced in the context of the MY34 GDS (Neary et al., 2020) or assimilated to explore the effect on escape rates of the MY34 regional C storm (Holmes et al., 2021). However, models have so far mainly focused on H atoms forming above 80 km or on particular dust storm events, leaving aside the question of the respective roles of the regular dusty perihelion climate and of isolated storms events (GDS, regional storms) in the escape budget.

The assumption that H production above 80 km dominates from an escape standpoint should be revisited by considering the nature of transport (advection, not diffusion) and the contribution of the atmosphere below. In that context, a different yet complementary perspective would look at the fate of a wet air parcel lifted from near the ground and progressively carried to an altitude range where H atoms are produced and then diffuse up the exobase. This supposes to adopt a Lagrangian standpoint, where one tracks over time (i.e., altitude) the changing gaseous composition inside the parcel and can better constrain the origin of the H atoms that populate the upper atmosphere.

To this end, we have employed a hybrid approach combining observational results, photochemistry and transport diagnostics from a 3D Mars climate model to represent the processes affecting the composition of an air parcel over time. The rationale for this simplified approach is that the entire representation of H production, evolution, and transport cannot be based solely on observations or the 3D model. This approach of mixing observations and model results together to infer production of hydrogen in the Martian atmosphere was introduced by Alday et al. (2021) who established the prevalence of the southern spring/summer in the annual H production of the middle atmosphere.

Observations can only indirectly constrain the velocity of ascent in the middle atmosphere, but they can constrain directly water vapor, pressure and temperature, which are the main parameters to model the relevant photochemistry. On the other hand, given the current maturity of Mars climate models (Navarro et al., 2014; Haberle et al. 2019; Shaposhnikov et al. 2019; Neary et al., 2020; Shaposhnikov et al. 2022), using their transport diagnostics is a

relevant option for specifying the range of vertical wind speeds needed for our model. An assimilation method like the one presented in Holmes et al. (2021) constitutes another way to merge observations and theory and explore the mechanisms subtending an observed atmospheric state. However, the loose coverage of TGO solar occultations (only two specific latitudes can be observed on any given day) is a strong limitation for an assimilation framework, and it is unclear how much such sparse observations can contribute to establishing an assimilated atmospheric state at very high altitude.

Our hybrid model tracks the fate of a wet atmospheric parcel undergoing ascent and chemistry, using the observed water vapor profiles reported in Belyaev et al. (2021) and the chemical model of Lefèvre et al. (2004) whose latest version has been presented in Lefèvre et al. (2021). We aim at tracking the variation in H number density ($N_H$) inside the parcel during its ascent to the upper atmosphere at times of intensified upward transport, i.e., during perihelion and during the MY34 GDS. The parcel ascends at a velocity $\omega$ of 10 cm/s as derived from the Mars Climate database (Millour et al., 2017, see Figure 1). Compared to the eddy mixing coefficient used in Chaffin et al. (2017), the upward motion predicted by the MCD is equally fast, since:

$$\tau_{adv} = H / \omega \quad = 10^5 \text{ s (~1 martian day)}$$

$$\tau_{diff} = H^2 / k_{diff} = 10^5 \text{ s}$$

where H is the atmospheric scale height (~10 km), and $k_{diff}$ is the eddy mixing coefficient ($10^7$ $cm^2/s$, see Chaffin et al., 2017 and Krasnopolsky, 2019). The typical variation of water vapor observed by NGIMS indicates that the abundance of ionized by-products of $H_2O$ were multiplied by 2 to 3 over ~2 days at 150 km, supporting our assumption for $\omega$.

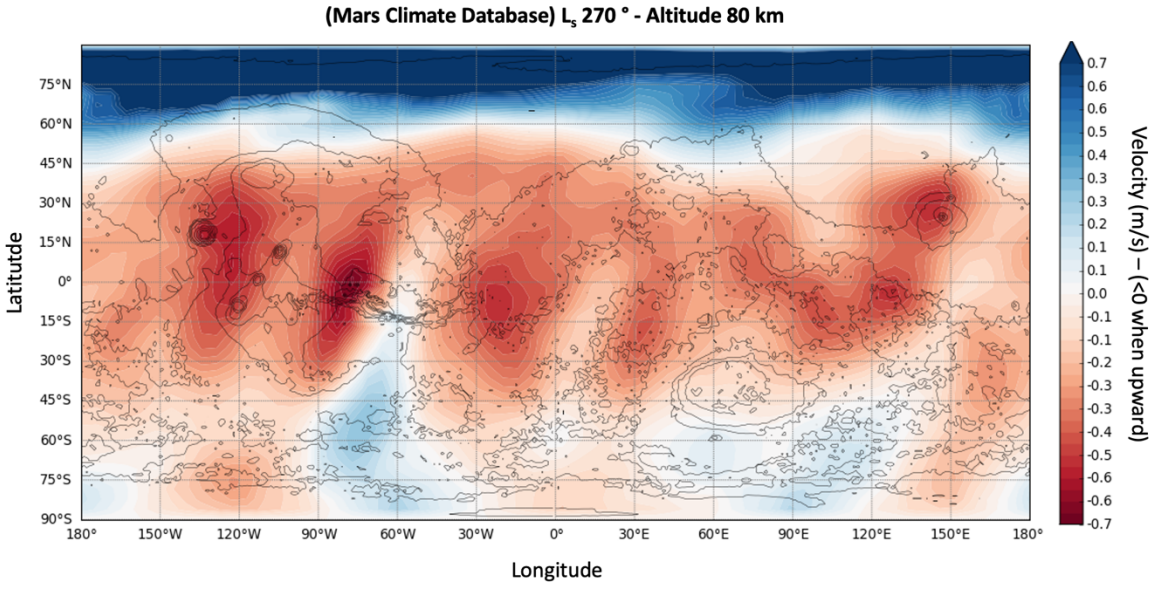


*Figure 1: Vertical velocity as a function of longitude and latitude extracted from the climatological scenario of the Mars Climate Database at $L_s$ 270°, an altitude of 80 km and noon time everywhere (Millour et al., 2017). Velocity is expressed in m/s (the maximum value is +1.7 m/s). Negative values (in red) denote upward orientation. http://www-mars.lmd.jussieu.fr/mcd_python/*

However, to address the sensitivity of our results to vertical speed, we also tested model response to velocities ranging from 1 to 50 cm/s as described thereafter. The vertical domain goes from the surface up to 100 km. At every time step, the concentration of water vapor inside the parcel is set to that observed by ACS at the same altitude (Belyaev et al., 2021). A net

budget of H atoms added/removed to/from the system is then computed by integrating H loss and production rates. H net production is only due to $H_2O$ photolysis, while its loss is mostly due to reactions with $O_3$, $HO_2$, and $O_2$ (Nair., 1994). Photochemical reaction rates used in our model to determine the net production of H atoms in the parcel at every 10-meter step of its ascent were computed offline and consist of diurnal averages for the $L_s$ considered. We did not include ionized chemistry, which is only relevant in the ionosphere (>100 km), that is located above the upper boundary of our model domain. Because the air parcel pressure decreases during its ascent, a dilution resulting from the pressure reduction induced by the parcel volume expansion between two adjacent levels is also applied to $N_H$.

## 3 Results

### 3.1 Periodic and stochastic events

One can distinguish between two modes of high-altitude water vapor migration: periodic and stochastic. The periodic mode relates to perihelion conditions as it occurs every year at the same period of time and is only driven by the reproducible evolution of the southern spring/summer climatic conditions, except when affected by the occurrence of a GDS such as in MY28. The stochastic mode corresponds to the unpredictable occurrences of dust storms, whose impact on climate is large-scale. This concerns global dust storms, and large-scale A-, B-, C- storms. Both periodic and stochastic modes occur only during the second half of the year, and it is now widely accepted that only southern spring and summer contribute to water vapor migration to the upper atmosphere (Alday et al., 2021).

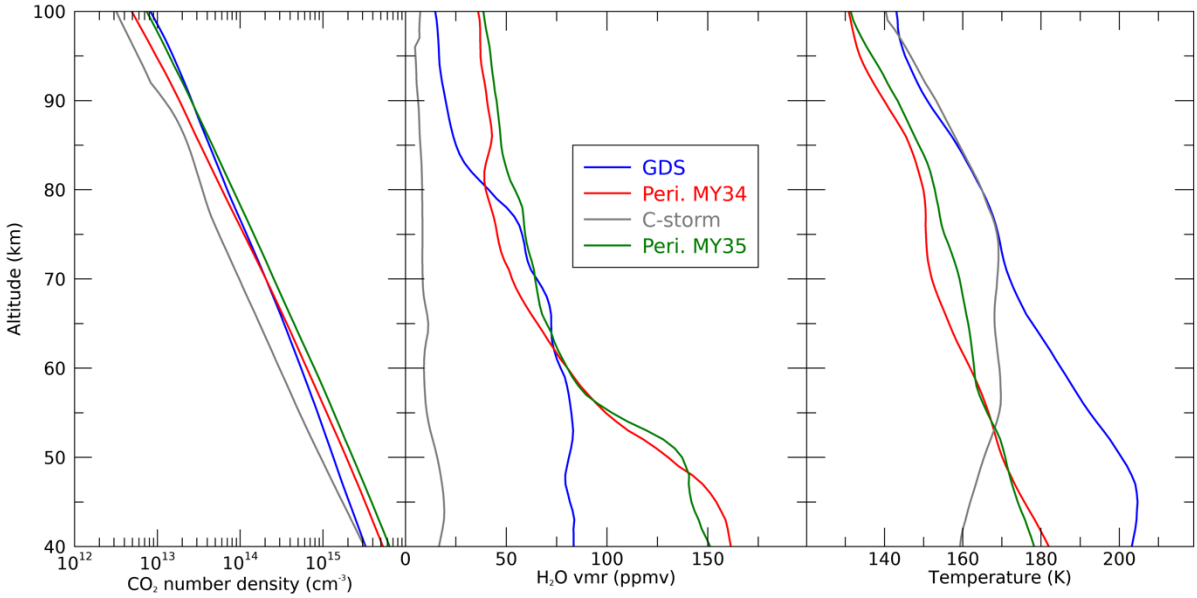


*Figure 2: $CO_2$ number density, $H_2O$ relative abundance and temperature derived from ACS data by Belyaev et al. (2021) for the four cases investigated in this study: MY34 GDS, Perihelion and C-storm, MY35 Perihelion. The smaller water abundance of the C-storm is potentially the result of an observational gap in ACS data.*

The relative importance of each mode in the long-term escape of water has been subject to debate. The main question that is addressed here is how powerful and frequent each mode of water upsurge is. All modes are characterized by sharp rises of water vapor, yet they differ in the way the atmosphere controls these rises. For instance, the MY34 GDS occurred at a time when the equinoctial circulation dominates, with a dual cell pattern centered about the equator where the rising region is thus located (Neary et al., 2020; Shaposhnikov et al., 2022). In contrast, the rise occurring around perihelion coincides with the southern solstice circulation

pattern, with a single cell whose rising branch is positioned in the mid-to-high southern latitudes. The strength of the southern spring/summer circulation pattern is boosted by the warmer perihelion climate and the topographic dichotomy (Richardson and Wilson, 2002).

Following the distinction between stochastic and periodic modes of water transfer, we selected the same periods of time as Belyaev et al. (2021) to which we added the MY34 C-storm period from the same dataset (see Figure 2). We thus based our simulations on data collected during perihelion (Ls 270°) in MY34 and MY35, as well as during the MY34 C-storm (Ls 330°), and during the climax of the MY34 GDS (195°-220°).

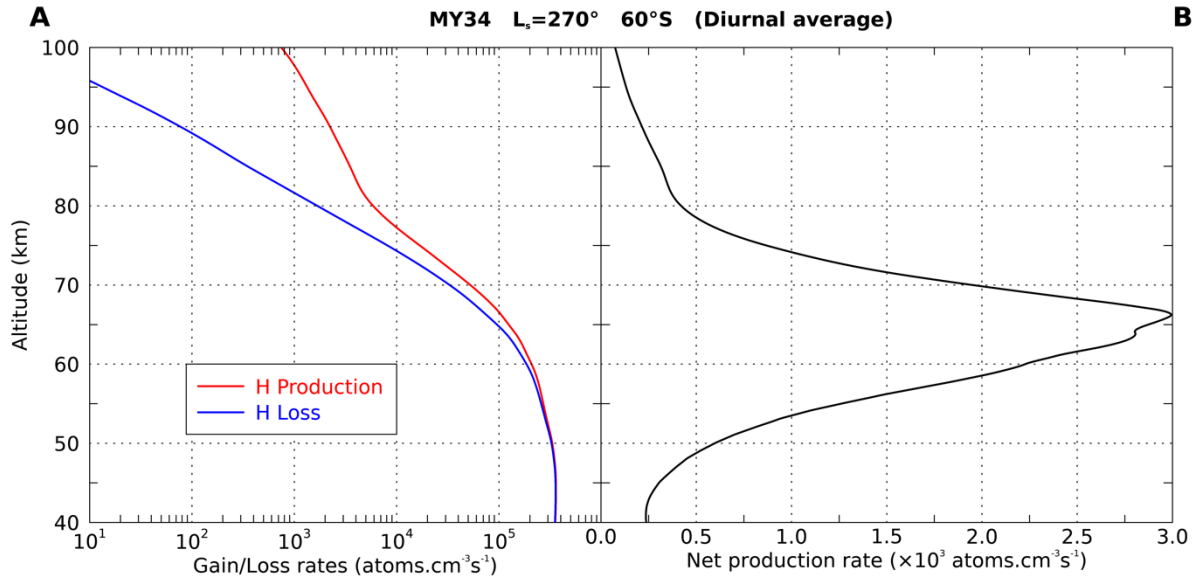


*Figure 3: (A) H production and loss rates as predicted by a photochemical model for the MY34 Perihelion case, using pressure, temperature, and water vapor profiles obtained by ACS MIR channel. H production is only due to water vapor photolysis. H loss relies on reactions with $O_3$, $HO_2$, and $O_2$. (B) H net budget calculated by subtracting loss from production rates.*

For simplicity, we assume that each simulation is representative of the transport and thermodynamical conditions encountered by water for each period of interest. Therefore, we conducted four simulations. Results were obtained for a particular latitude range that theoretically corresponds to the main zone of H ascent (i.e., 60°S for Perihelion and C-Storm, 0° for the GDS).

## 3.2 MY34 Perihelion

Here we consider the particular situation occurring during the transition between southern spring and summer and that is henceforth referred to as the Perihelion season and that encompasses the period from $L_s$ 240° to 270°. Alday et al. (2021) demonstrated the prevalence of the Perihelion season for the formation of H and D atoms at 60 km of altitude. This conclusion was based on applying theoretical photolysis rates upon HDO and $H_2O$ profiles observed by ACS.

### 3.2.1 Timescale Consideration

Figure 3-A shows that H chemical loss balances photolysis production up to ~50 km, above which production dominates loss increasingly with altitude. Therefore, H atoms can only ascend if they are produced above 50 km. The net production rate (Figure 3-B) peaks at ~65 km since, at the same time, the number density of water vapor from which H is directly produced declines with pressure. H atoms produced below 60 km do not contribute to the transfer of H

to the upper atmosphere above 80 km, since loss operates >10 times faster than advection (hours vs. days, see Figure 4), as explained in Section 3.4.

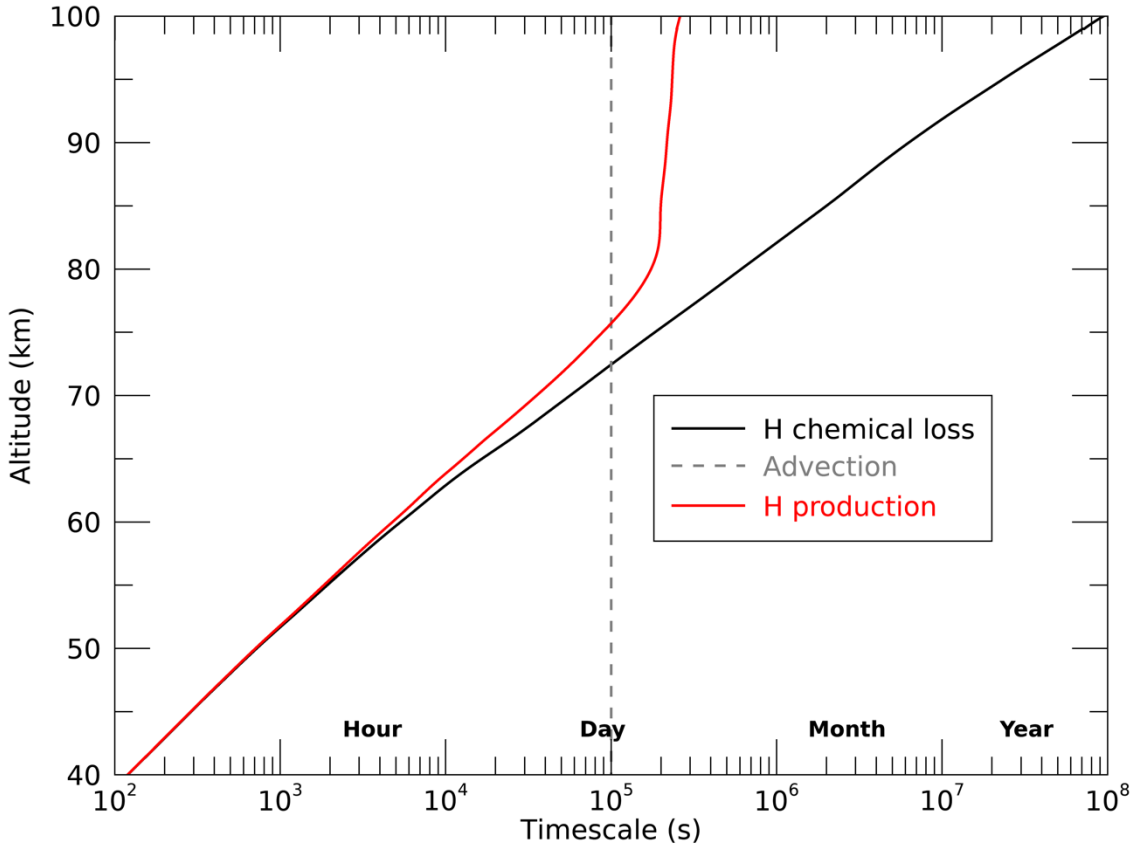


*Figure 4: Timescales associated with the various processes represented in the air parcel model, transport timescale is deduced from an ascent velocity of 10 cm/s.*

### 3.2.2 Hydrogen origin in the lower atmosphere

Our air parcel model can be used to track the origin of the H atoms advected to 80 km (Figure 5). To do so, we restrict production inside 5-km atmospheric layers located between 40 and 80 km (Figure 5). Our model confirms that no H atoms produced below 60 km can access the upper atmosphere as it is bound to recombine before reaching 80 km, which implies that almost no atoms produced in the peak production region contribute to escape. After being advected from their production zone below 60 km, H atoms are completely lost after 1 or 2 km of ascent. The production zone that matters for escape comprises altitudes from 65 to 80 km, with a dominant contribution from the 70 to 75 km region.

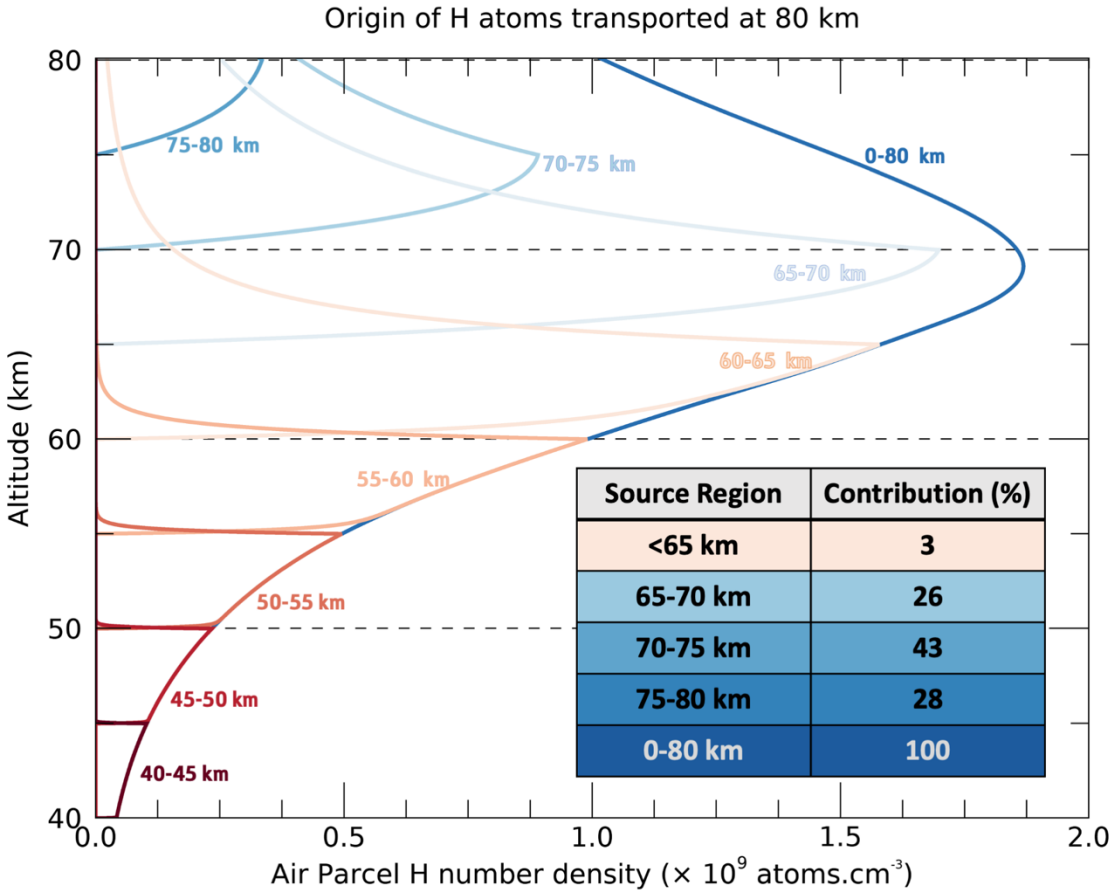


*Figure 5: Air parcel model predictions for a set of configurations where production only occurs in a 5 km-thick layer whose top altitude we vary from 45 to 80 km. Plotted quantity is the H number density (atoms.cm$^{-3}$) in the parcel. The shape of each curve reflects the processes at work inside the parcel during its ascent at 10 cm/s. Below 55 km, H is instantaneously lost after leaving its production zone. Then, its increasing lifetime allows it to ascend several km before destruction. Above 60 km, an increasing fraction of the produced atoms can be advected up to 80 km. The contribution of each 5 km layer is calculated by dividing their corresponding $N_H$ at 80 km with that of the 0-80 km case, that is the nominal full production case.*

### 3.2.3 Upward Flux

Figure 6 shows the altitude (or equivalently time, on the right axis) evolution of the hydrogen number density ($N_H$) in the air parcel and the corresponding upward flux (equal to $N_H \times \omega$). $N_H$ shows a pronounced peak of $1.9 \times 10^9$ atoms.cm$^{-3}$ at 69 km that is reminiscent of the net production peak found at 65 km. However, as explained earlier, $N_H$ then decreases after rising above the peak as subsequent H production diminishes and cannot compensate dilution subsequent to the parcel volume expansion.

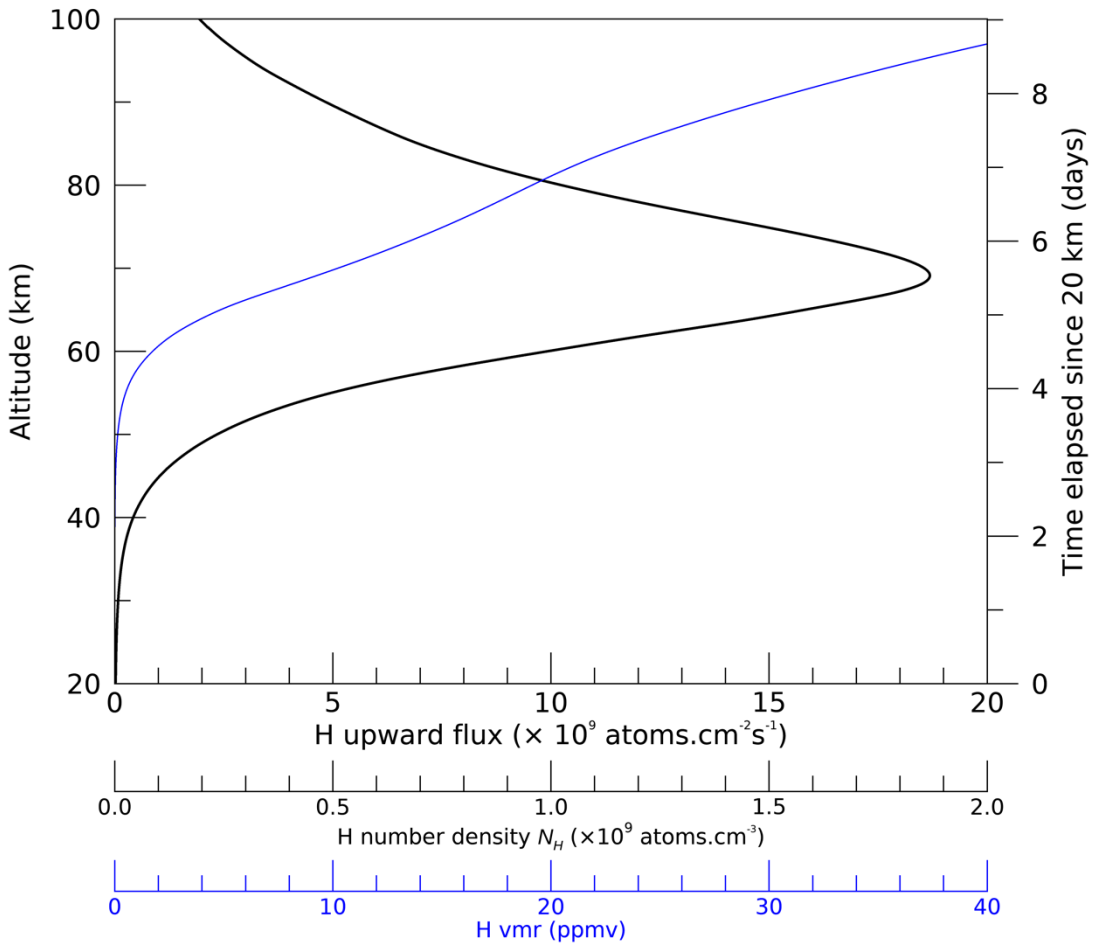


*Figure 6: Model results for the H number density in the parcel ($N_H$) and the resulting upward flux for the MY34 perihelion case (black solid line). Contrasting with the $N_H$ profile and its pronounced peak at 70 km, the H volume mixing ratio (vmr) profile (blue line) exhibits a constant increase from 55 km up to 100 km. Note that the 1.1 × $10^{10}$ $cm^{-2}s^{-1}$ flux value found at 80 km is nearly 50 times greater than the canonical escape rate of ~2 ×$10^{8}$ $cm^{-2}s^{-1}$deduced from $H_2$ dominated formation of upper atmospheric H (Krasnopolsky, 2019; Stone et al., 2020).*

At 80 km, we find that the upward hydrogen flux is of 1.1 × $10^{10}$ $cm^{-2}s^{-1}$, a value that is nearly twice the net photolysis product of H integrated from 80 to 100 km. The H flux at the bottom of the upper atmospheric domain is not only significant, it actually accounts for a dominant portion of the H budget in the upper atmosphere of the southern summer, when H is known to escape massively.

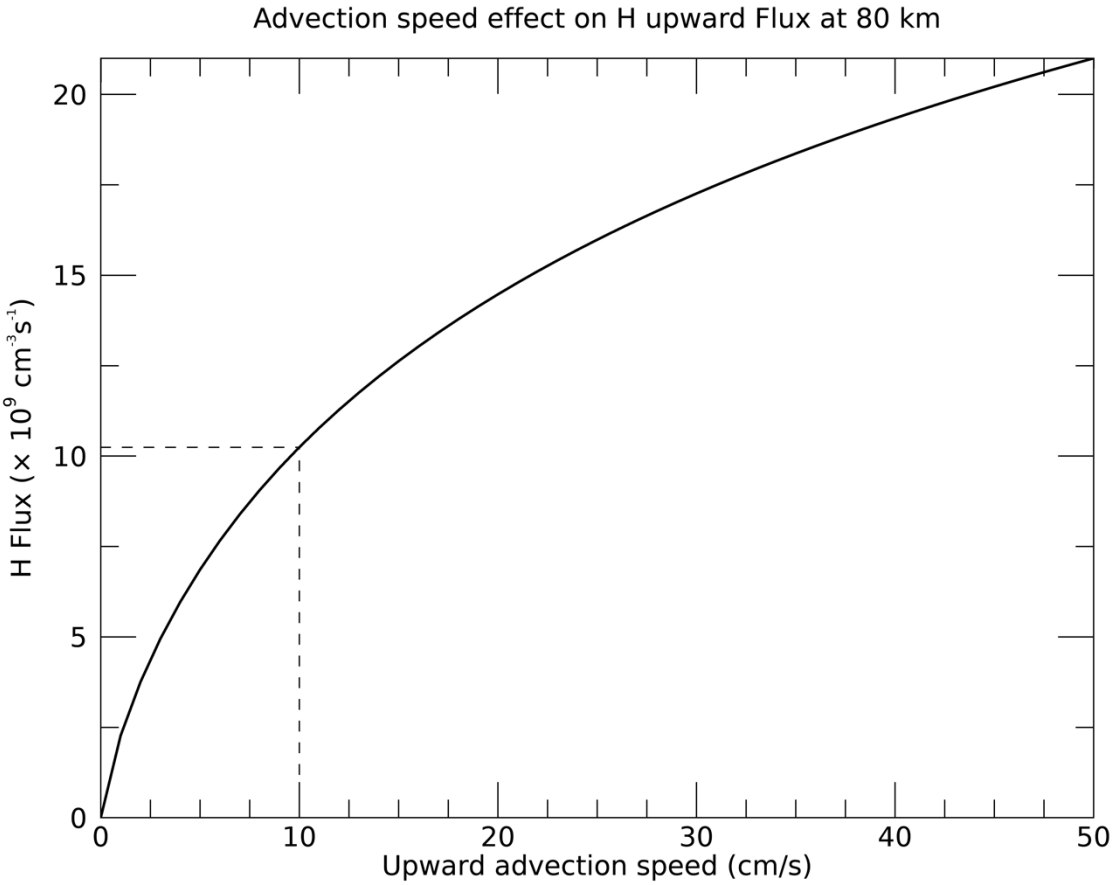


*Figure 7: Sensitivity of the simulated H flux at 80 km to upward velocity in the case of the MY34 Perihelion simulation. Our baseline has a velocity of 10 cm/s, yet even a twofold increase or decrease in velocity only impacts H flux by ~40%.*

#### 3.2.4 Sensitivity to ascent speed

At an upward speed of 10 cm/s, it takes roughly a day for the parcel to ascend 10 km in altitude. The derived H flux at a given altitude being the product of ascent speed with the H number density in the parcel, a change in speed linearly affects this product. However, it also indirectly affects it through the H number density in the parcel. Indeed, $N_H$ is history-dependent, as it integrates over time the effects of local conditions on loss and production in the parcel. In turn, the effect of local conditions on H budget depends on the residence time of the parcel at a given altitude, and thus on its ascent speed. Therefore, a higher ascent speed also implies the parcel spends less time in regions where it can accumulate H atoms.

This antagonism of effects explains the parabolic shape of the H flux dependence to ascent speed, as displayed in Figure 7, and additionally give our results on the 80 km H flux some immunity to speed uncertainty.

### 3.3 Other cases

#### 3.3.1 Result Comparison

The MY34 configuration described above has revealed the main characteristics of the H migration phenomenon, showing the significance of the H flux at 80 km and the partitioning of the H origin among the atmospheric layers located below and in particular between 60 and

80 km. We then subsequently applied our model to the three other configurations of interest: MY35 Perihelion, MY34 GDS and MY34 C-storm (see Figures 2 and 8). It is to be noted that a large part of the C-storm was not monitored by ACS due to TGO's orbit constraints. The data gap actually covers the peak activity of this regional storm, which implies our results underestimate the C-storm upward flux, since its water vapor profile exhibits distinctly smaller abundances compared to other cases (Figure 2). Yet, this event produced an intense brightening of the hydrogen corona (Chaffin et al., 2021).

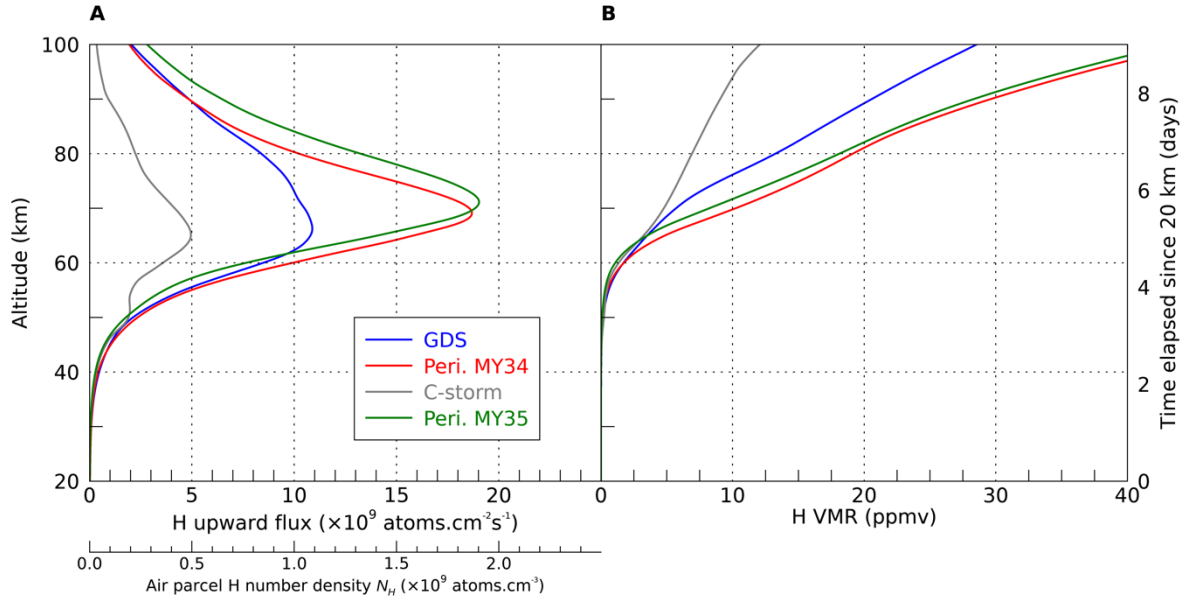


*Figure 8: A synthesis of the four configurations explored with the air parcel model: GDS, MY34 and MY35 Perihelion, MY34 C-storm. (A) H Upward flux and concentration in the parcel during its rise from 20 to 100 km. (B) Same as (A) except $N_H$ is converted into H vmr (ppmv).*

MY34 and MY35 Perihelion cases are in remarkable agreement, both exhibiting the same upward flux profile (Figure 8) with a pronounced peak around 70 km only slightly shifted upward in MY35. This altitude offset explains why the MY35 80 km H flux is ~30% larger than MY34, as a higher proportion of H atoms are produced closer to the 80 km boundary. Indeed, water vapor is 15 ppmv more abundant in MY35 at 80 km, which then directly impacts H production and upward flux (Figure 2). These results support the idea that the perihelion configuration is highly reproductible from year to year, which provides confidence for extrapolating its contribution in the escape budget on a longer term.

The GDS case exhibits a H flux profile that is significantly flared compared to the perihelion case, reflecting the distinct $H_2O$ vmr profile of the GDS that shows a nearly uniform mixing ratio of ~70 ppmv below 70 km. The GDS H flux has a maximum value located at 65 km that is twice smaller than for perihelion cases. At 80 km, GDS flux remains distinctly smaller than the two perihelion seasons considered here. However, at 85 km, the GDS flux catches up with MY34 Perihelion flux. The broadened peak of the GDS implies that a larger proportion (~50%) of the H population origin is located close to the 80 km boundary. In addition, the total density of the MY34 GDS above 80 km is higher than for perihelion cases (Figure 2), which mitigates the volume expansion (dilution) effect on the air parcel in this altitude range.

### 3.3.2 Upward flux vs. neutral photolysis above 80 km

Considering that other processes are at work above 80 km, it is interesting to determine how the upward H flux at 80 km compares, in terms of hydrogen input into the region above 80 km, with these other processes. One of them is the direct deposition of hydrogen from water photolysis above 80 km. We mentioned earlier that in the case of MY34 perihelion, the upward flux was about twice the net column production of H atoms out of photolysis between 80 and 100 km. We expanded this comparison to all other cases and found the following: (i) for MY35 perihelion, the upward flux was 55% greater than local photolysis production, (ii) for the MY34 GDS, the upward flux was 30% greater, and (iii) for the MY34 C-storm, the upward flux was nearly three times higher than local production.

These results imply that the upward influx of H at the bottom of the upper atmospheric domain is the dominant supplier in the context of the neutral photochemistry.

### 3.3.3 Upward flux vs. ionized chemistry

Without water at high altitude, H is only produced out of the reaction between $CO_2^+$ and $H_2$, leading to a column production rate of the order of $1.6 \times 10^8$ $cm^{-2}s^{-1}$ (Krasnopolsky, 2019). This $H_2$ chemical path supplies a background of H atoms all year long that is independent of the quantity of water vapor in the upper atmosphere.

However, Krasnopolsky (2019) completed the $H_2$ pathway with ionized chemistry involving water and triggered by $H_2O$ reacting with $CO_2^+$. He estimated that water chemistry in the thermosphere was producing H at a rate equal to:

$$\varphi_{H\uparrow} \ (cm^{-2}s^{-1}) = 1.6 \times 10^8 + 1.4 \times 10^7 \, f_{H2O}{}^*(ppm)$$

which, in the case water has 60 ppmv relative abundance at 80 km, yields an H escape rate of $10^9$ $cm^{-2}s^{-1}$.

Stone et al. (2020) describe a series of high altitude (150 km) NGIMS in situ measurements of ionized water by-products that they used as a proxy to estimate water vapor local concentration. They then applied an ionized chemistry model similar to Krasnopolsky (2019) to infer the production of H atoms out of $H_2O$ reactions with $CO_2^+$. These authors found a net production rate of $2.8 \times 10^9$ $cm^{-2}s^{-1}$.

The difference of results between these two studies is not easily tractable, yet may be explained by the fact that Stone et al. (2020) directly constrained their model with NGIMS measurements that probed the ion composition of the atmosphere down to ~125 km during a MAVEN deep dip, and possibly because they employed updated reaction rates compared to Krasnopolsky (2019). Yet, both rely on the same approach and concur on the fact that ionized chemistry of water dominates over $H_2$ chemistry and is a major supplier of escaping H atoms at times of "high water". Stone et al. (2020) further advocated that MY34 GDS produced such a change in the ion by-products of water that GDS are likely to represent the main escape process for water overall.

### 3.3.4 Implication for escape

Assuming that the H atoms crossing the 80 km boundary can be then carried up to escape altitudes, our results shed light on the potential of each event for hydrogen escape. Table 1 summarizes the production rates computed for most of the events discussed here and for the various H production modes that have been studied so far. Of all the processes involved in the production and injection of H atoms into the upper atmosphere, the upward transfer is found to be systematically greater than production from water photolysis or ionized chemistry.

This statement is only valid outside the cold aphelion period, where $H_2$ molecules are the main precursor of H atoms.

| **H production type** in column rate (atoms per $cm^{-2}s^{-1}$) | | **Event type** | | |
|---|---|---|---|---|
| | | **Perihelion MY34 / MY35** | **Global Dust Storm** | **C-storm** |
| **$H_2$-$CO_2^+$ chemistry** | | $1.6 \times 10^8$ (k19) | $1.6 \times 10^8$ (k19) | $1.6 \times 10^8$ (k19) |
| **$H_2O$-$CO_2^+$ chemistry** | | $1 \times 10^9$ (k19) | $2.38 \times 10^9$ (s20) | |
| **This study** | **$H_2O$ photolysis (80-100 km)** | $5 \times 10^9$ / $7.5 \times 10^9$ | $5.4 \times 10^9$ | $7 \times 10^8$ |
| | **H upward flux** | $1 \times 10^{10}$ / $1.3 \times 10^{10}$ | $8.4 \times 10^9$ | $2.2 \times 10^9$ |

*Table 1: a synthesis of the results obtained in this study and compared with other works (k19: Krasnopolsky, 2019; s20: Stone et al., 2020).*

This raises the question of the fate of H atoms crossing the 80 km boundary. Shaposhnikov et al. (2022) explore the dynamical mechanisms that carry volatiles into the upper atmosphere at GDS and perihelion times. Using a Mars' GCM to address the gravity wave breaking effect on global circulation and the transport of water at high altitude, they show that atmospheric updrafts are the main carrier of volatiles up to 100 km, above which molecular diffusion combines with advection and then controls above 120 km the ascent of gases to the exobase. It is therefore legitimate to apply our advective transport model to hydrogen atoms produced below 80 km. Since the lifetime of hydrogen atoms increases steadily with altitude, once they have entered the upper atmospheric domain above 80 km, they are likely to reside there long enough for a significant fraction of them to reach the exobase. In fact, the way circulation is organized at times of high water events implies a massive upwelling either at the equator (GDS) or at high southern latitudes (perihelion) compensated by a massive downwelling at the pole(s). Figure 1 gives a good illustration of the upwelling and downwelling effects on the vertical velocity field. During perihelion, downwelling velocity is twice larger than upwelling (1.7, not shown, vs. 0.7 m/s maximum values) yet is confined into a narrow band at the north pole. Our air parcel concept only captures the ascent part of the hydrogen journey into the upper atmosphere. At 100 km, that is at the top of our model, molecular diffusion will then take over the rest of the ascent that will lead released H atoms to escaping altitude. Yet a fraction of these atoms will eventually return to the middle atmosphere via the downwelling region.

Depending on the value of this fraction, our model for direct H injection into the upper atmosphere consequently appears as a plausible dominant contributor to H escape overall. At least, the upward transport of H atoms is comparable in strength with the direct deposition of H atoms from water photolysis above 80 km. This consideration is in line with the Chaffin mechanism, except our study allows disentangling the role and contribution of its principal components, namely transport from the middle atmosphere and production by photolysis.

#### 3.3.5 Perihelion: the preferred period for H escape?

Our comparison found a very consistent behavior of the H flux around perihelion for two consecutive years. It is premature to conclude on the role of the GDS on the long-term escape of water, considering that the MY34 GDS was a particular type of GDS (yet replicating

the time period of the MY25 GDS) which have been observed at other times in the Southern spring and summer (the MY28 GDS started at $L_s$ 270°). However, within the framework and constraints of this study, we find that the perihelion period supplies on any given year at least as much as the GDS did in MY34. Considering that GDS have been observed to occur every >3 Martian years, on the long term (that is within the shortest of the orbital cycle), perihelion likely remains the dominant season for conveying H atoms in the upper atmosphere, thereby imprinting a dominant effect on escape. On top of it, regional storms shall add to this hydrogen transfer. Their relative importance is more difficult to evaluate, as only a fraction of a single event (the 2018 C-storm) could be tested with our model, which delivered results arguably underestimating the H flux.

There are however reasons to argue that perihelion climate controls the transfer of H overall. First, the warmer and dustier conditions of the perihelion climate last ~60° $L_s$, a duration comparable to GDS' and which is greater than the duration of regional storms. Second, perihelion corresponds to the seasonal maximum in the strength of the global Hadley circulation, which is additionally boosted by the topographic dichotomy. Third, the higher solar input of perihelion implies that a smaller amount of dust is needed to produce the same warming as extra-perihelion events. In contrast, the effect of regional storms on H upward flux relies on how much dust regional storms do lift, which is variable from year to year as shown in the climatology of dust column opacity (see Figure 16 in Montabone et al., 2015).

## 4 Conclusion

We have used a 1D hybrid model to represent the ascent of a wet air parcel at times of intense dust and transport activity. This model combines observations of the ACS instrument onboard TGO that measured, for the first time, water vapor abundance from 20 to 120 km (Belyaev et al., 2021). These observations enable the in-depth study of how the water vapor penetration to high altitude contributes to hydrogen production above 80 km. In contrast with other 1D models that have been used to explore Mars' photochemistry, our model does not represent the vertical transport through the standard eddy diffusion but through advection with a constant velocity of 10 cm/s up to 100 km. This choice more faithfully represents the way air masses are elevated during periods of high water events and intensified circulation.

We then combined the air parcel advection with ACS water vapor measurements and a detailed model of the neutral photochemistry to track the H concentration (or number density) in the parcel during its ascent. We find the production and further advection of H atoms from 60 to 80 km supply an upward flux of hydrogen that overwhelms all other modes of hydrogen production in the upper atmosphere. The upward flux shows a slight dependence on the ascent velocity, which thus mitigates the importance of specifying the correct velocity when comparing different events together.

Our results imply that, contrary to a common assumption made in models used to study Mars' photochemistry and escape processes, the region between 60 and 80 km cannot be neglected in the production and migration of hydrogen to the upper atmosphere. In particular, these results imply that upper atmosphere photochemistry models intending to capture Southern Summer conditions need to carefully consider the flux boundary condition for H at the lower boundary if it is higher than 80 km.

Testing a variety of configurations, from the MY34 GDS to the recent MY35 perihelion period, we have been able to assess how the hydrogen upward flux from above 60 km varies with events. Stochastic events (GDS and A, B, C- storms) have a strong imprint on the escape budget, but our results suggest perihelion remains the dominant escape component on the long term.

**Acknowledgements**

ExoMars is the space mission of ESA and Roscosmos. The ACS investigation was developed by the Space Research Institute (IKI) in Moscow, and the Laboratoire Atmospheres, Milieux, Observations Spatiales (LATMOS) in Guyancourt. The investigation was funded by Roscosmos, the National Centre for Space Studies of France (CNES) and RSF (Russian Science Foundation 20-42-0903). This work was funded by CNES, the Agence Nationale de la Recherche (ANR, PRCI, CE31 AAPG2019, MCUBE project), DIM ACAV labelled by the Ile-de-France region in support for the research (Domaine d'Intérêt Majeur, Astrophysique et Conditions d'Apparition de la Vie)".

**Data availability**

The ACS data used in this study are published in Belyaev et al. (2021) and can be found at https://data.mendeley.com/datasets/995y7ymdgm/draft?a=daa72362-898d- 4c86-8a13-023b4b59134c.
The data produced by our model can be obtained (for review purpose) on the following link: https://mycore.core-cloud.net/index.php/s/na60fDZRoNCGa6i
These data will be deposited after the review on the ESPRI/IPSL archive server, at which point a doi will be created.

**References**

Alday, J., Trokhimovskiy, A., Irwin, P. G. J., Wilson, C. F., Montmessin, F., Lefévre, F., et al. (2021). Isotopic fractionation of water and its photolytic products in the atmosphere of Mars. Nature Astronomy. https://doi.org/10.1038/s41550-021-01389-x

Aoki, S., Vandaele, A. C., Daerden, F., Villanueva, G. L., Liuzzi, G., Thomas, I. R., et al. (2019). Water Vapor Vertical Profiles on Mars in Dust Storms Observed by TGO/NOMAD. *Journal of Geophysical Research: Planets*, *124*(12), 3482–3497. https://doi.org/10.1029/2019JE006109

Belyaev, D. A., Fedorova, A. A., Trokhimovskiy, A., Alday, J., Montmessin, F., Korablev, O. I., et al. (2021). Revealing a High Water Abundance in the Upper Mesosphere of Mars With ACS Onboard TGO. *Geophysical Research Letters*, *48*(10). https://doi.org/10.1029/2021GL093411

Carr, M. H. (1987). Water on Mars, *326*, 30–35. https://doi.org/10.1038/326030a0

Chaffin, Michael S., Chaufray, J.-Y., Stewart, I., Montmessin, F., Schneider, N. M., & Bertaux, J.-L. (2014). Unexpected variability of Martian hydrogen escape: *Geophysical Research Letters*, *41*(2), 314–320. https://doi.org/10.1002/2013GL058578

Chaffin, M. S., Deighan, J., Schneider, N. M., & Stewart, A. I. F. (2017). Elevated atmospheric escape of atomic hydrogen from Mars induced by high-altitude water. *Nature Geoscience*, *10*(3), 174–178. https://doi.org/10.1038/ngeo2887

Chaffin, M. S., Kass, D. M., Aoki, S., Fedorova, A. A., Deighan, J., Connour, K., et al. (2021). Martian water loss to space enhanced by regional dust storms. *Nature Astronomy*, *5*(10), 1036–1042. https://doi.org/10.1038/s41550-021-01425-w

Clancy, R. T., Grossman, A. W., Wolff, M. J., James, P. B., Rudy, D. J., Billawala, Y. N., et al. (1996). Water vapor saturation at low latitudes around aphelion: A key to Mars climate? *Icarus*, *122*, 36–62.

575 Clarke, J. T., Bertaux, J.-L., Chaufray, J.-Y., Gladstone, G. R., Quemerais, E., Wilson, J. K.,
576 & Bhattacharyya, D. (2014). A rapid decrease of the hydrogen corona of Mars: the
577 Martian Hydrogen Corona. Geophysical Research Letters, 41(22), 8013–8020.
578 https://doi.org/10.1002/2014GL061803
579 Davies, D. W. (1979). The vertical distribution of Mars water vapor. *Journal of Geophysical*
580 *Research*, *84*(B6), 2875. https://doi.org/10.1029/JB084iB06p02875
581 Fedorova, A. A., Korablev, O. I., Bertaux, J.-L., Rodin, A. V., Montmessin, F., Belyaev, D.
582 A., & Reberac, A. (2009). Solar infrared occultation observations by SPICAM
583 experiment on Mars-Express: Simultaneous measurements of the vertical distributions
584 of H2O, CO2 and aerosol. *Icarus*, *200*(1), 96–117.
585 https://doi.org/10.1016/j.icarus.2008.11.006
586 Fedorova, A., Bertaux, J.-L., Betsis, D., Montmessin, F., Korablev, O., Maltagliati, L., &
587 Clarke, J. (2018). Water vapor in the middle atmosphere of Mars during the 2007 global
588 dust storm. *Icarus*, *300*, 440–457. https://doi.org/10.1016/j.icarus.2017.09.025
589 Fedorova, A. A., Montmessin, F., Korablev, O., Luginin, M., Trokhimovskiy, A., Belyaev,
590 D. A., et al. (2020). Stormy water on Mars: The distribution and saturation of
591 atmospheric water during the dusty season. *Science*, *367*(6475), 297–300.
592 https://doi.org/10.1126/science.aay9522
593 Fedorova, A., Montmessin, F., Korablev, O., Lefèvre, F., Trokhimovskiy, A., & Bertaux, J.
594 (2021). Multi-Annual Monitoring of the Water Vapor Vertical Distribution on Mars by
595 SPICAM on Mars Express. *Journal of Geophysical Research: Planets*, *126*(1).
596 https://doi.org/10.1029/2020JE006616
597 Haberle, R. M., Kahre, M. A., Hollingsworth, J. L., Montmessin, F., Wilson, R. J., Urata, R.
598 A., et al. (2019). Documentation of the NASA/Ames Legacy Mars Global Climate
599 Model: Simulations of the present seasonal water cycle. *Icarus*, *333*, 130–164.
600 https://doi.org/10.1016/j.icarus.2019.03.026
601 Heavens, N. G., Kleinböhl, A., Chaffin, M. S., Halekas, J. S., Kass, D. M., Hayne, P. O., et
602 al. (2018). Hydrogen escape from Mars enhanced by deep convection in dust storms.
603 *Nature Astronomy*, *2*(2), 126–132. https://doi.org/10.1038/s41550-017-0353-4
604 Holmes, J. A., Lewis, S. R., Patel, M. R., Chaffin, M. S., Cangi, E. M., Deighan, J., et al.
605 (2021). Enhanced water loss from the martian atmosphere during a regional-scale dust
606 storm and implications for long-term water loss. *Earth and Planetary Science Letters*,
607 *571*, 117109. https://doi.org/10.1016/j.epsl.2021.117109
608 Jakosky, B. M., Brain, D., Chaffin, M., Curry, S., Deighan, J., Grebowsky, J., et al. (2018).
609 Loss of the Martian atmosphere to space: Present-day loss rates determined from
610 MAVEN observations and integrated loss through time. *Icarus*, *315*, 146–157.
611 https://doi.org/10.1016/j.icarus.2018.05.030
612 Krasnopolsky, V. A. (2002). Mars' upper atmosphere and ionosphere at low, medium, and
613 high solar activities: Implications for evolution of water: Mars' upper atmosphere and
614 ionosphere. *Journal of Geophysical Research: Planets*, *107*(E12), 11-1-11–11.
615 https://doi.org/10.1029/2001JE001809
616 Krasnopolsky, V. A. (2019). Photochemistry of water in the martian thermosphere and its
617 effect on hydrogen escape. *Icarus*, *321*, 62–70.
618 https://doi.org/10.1016/j.icarus.2018.10.033

Lefèvre, F., Lebonnois, S., Montmessin, F., & Forget, F. (2004). Three-dimensional modeling of ozone on Mars. *Journal of Geophysical Research E: Planets*, *109*(7), E07004 1-20. https://doi.org/10.1029/2004JE002268

Lefèvre, F., Trokhimovskiy, A., Fedorova, A., Baggio, L., Lacombe, G., Määttänen, A., et al. (2021). Relationship Between the Ozone and Water Vapor Columns on Mars as Observed by SPICAM and Calculated by a Global Climate Model. Journal of Geophysical Research: Planets, 126(4). https://doi.org/10.1029/2021JE006838

Maltagliati, L., Montmessin, F., Fedorova, A., Korablev, O., Forget, F., & Bertaux, J.-L. (2011). Evidence of Water Vapor in Excess of Saturation in the Atmosphere of Mars. *Science*, *333*(6051), 1868–1871. https://doi.org/10.1126/science.1207957

Maltagliati, L., Montmessin, F., Korablev, O., Fedorova, A., Forget, F., Määttänen, A., et al. (2013). Annual survey of water vapor vertical distribution and water-aerosol coupling in the martian atmosphere observed by SPICAM/MEx solar occultations. *Icarus*, *223*, 942–962. https://doi.org/10.1016/j.icarus.2012.12.012

McElroy, M. B., & Donahue, T. M. (1972). Stability of the Martian Atmosphere. *Science*, *177*(4053), 986–988. https://doi.org/10.1126/science.177.4053.986

Millour, E., Forget, F., Spiga, A., Vals, M., Zakharov, A. V., Navarro, T., et al. (2017). The Mars Climate Database (MCD version 5.3). In *proceedings from the* 19th EGU General Assembly, EGU2017, 23-28 April, 2017 in Vienna, Austria, p. 12247.

Montabone, L., Forget, F., Millour, E., Wilson, R. J., Lewis, S. R., Cantor, B., et al. (2015). Eight-year climatology of dust optical depth on Mars. Icarus, 251, 65–95. https://doi.org/10.1016/j.icarus.2014.12.034

Nair, H. (1994). A Photochemical Model of the Martian Atmosphere. Icarus, 111(1), 124–150. https://doi.org/10.1006/icar.1994.1137

Navarro, T., Madeleine, J.-B., Forget, F., Spiga, A., Millour, E., Montmessin, F., & Määttänen, A. (2014). Global climate modeling of the Martian water cycle with improved microphysics and radiatively active water ice clouds. *Journal of Geophysical Research: Planets*, *119*(7), 1479–1495. https://doi.org/10.1002/2013JE004550

Neary, L., Daerden, F., Aoki, S., Whiteway, J., Clancy, R. T., Smith, M., et al. (2020). Explanation for the Increase in High-Altitude Water on Mars Observed by NOMAD During the 2018 Global Dust Storm. *Geophysical Research Letters*, *47*(7). https://doi.org/10.1029/2019GL084354

Parkinson, T. D., & Hunten, D. M. (1972). Spectroscopy and Aeronomy of O2 on Mars. *Journal of the Atmospheric Sciences*, *29*(7), 1380–1390. https://doi.org/10.1175/1520-0469(1972)029<1380:SAAOOO>2.0.CO;2

Richardson, M. I., & Wilson, R. J. (2002). A topographically forced asymmetry in the martian circulation and climate. *Nature*, *416*, 298–301.

Rodin, A., Korablev, O., & Moroz, V. (1997). Vertical Distribution of Water in the Near-Equatorial Troposphere of Mars: Water Vapor and Clouds. *Icarus*, *125*(1), 212–229. https://doi.org/10.1006/icar.1996.5602

Scheller, E. L., Ehlmann, B. L., Hu, R., Adams, D. J., & Yung, Y. L. (2021). Long-term drying of Mars by sequestration of ocean-scale volumes of water in the crust. *Science*, *372*(6537), 56–62. https://doi.org/10.1126/science.abc7717

Shaposhnikov, D. S., Medvedev, A. S., Rodin, A. V., & Hartogh, P. (2019). Seasonal Water "Pump" in the Atmosphere of Mars: Vertical Transport to the Thermosphere. *Geophysical Research Letters*, *46*(8), 4161–4169. https://doi.org/10.1029/2019GL082839

Shaposhnikov, D.S., Medvedev, A.S., Rodin, A.V., Yiğit, E., Hartogh, P., (2022). Martian Dust Storms and Gravity Waves: Disentangling Water Transport to the Upper Atmosphere. JGR Planets 127. https://doi.org/10.1029/2021JE007102

Stone, S. W., Yelle, R. V., Benna, M., Lo, D. Y., Elrod, M. K., & Mahaffy, P. R. (2020). Hydrogen escape from Mars is driven by seasonal and dust storm transport of water. *Science*, *370*(6518), 824–831. https://doi.org/10.1126/science.aba5229

Vandaele, A. C., Korablev, O., Daerden, F., Aoki, S., Thomas, I. R., Altieri, F., et al. (2019). Martian dust storm impact on atmospheric H2O and D/H observed by ExoMars Trace Gas Orbiter. *Nature*, *568*(7753), 521–525. https://doi.org/10.1038/s41586-019-1097-3